Environ Geol (2009) 58:1533–1540
DOI 10.1007/s00254-008-1654-9

ORIGINAL ARTICLE

Monitoring of land subsidence and ground fissures in Xian, China 2005–2006: mapped by SAR interferometry

C. Y. Zhao · Q. Zhang · X. L. Ding · Z. Lu · C. S. Yang · X. M. Qi

Received: 3 August 2008 / Accepted: 16 November 2008 / Published online: 6 January 2009

Abstract The City of Xian, China, has been experiencing significant land subsidence and ground fissure activities since 1960s, which have brought various severe geohazards including damages to buildings, bridges and other facilities. Monitoring of land subsidence and ground fissure activities can provide useful information for assessing the extent of, and mitigating such geohazards. In order to achieve robust Synthetic Aperture Radar Interferometry (InSAR) results, six interferometric pairs of Envisat ASAR data covering 2005–2006 are collected to analyze the InSAR processing errors firstly, such as temporal and spatial decorrelation error, external DEM error, atmospheric error and unwrapping error. Then the annual subsidence rate during 2005–2006 is calculated by weighted averaging two pairs of D-InSAR results with similar time spanning. Lastly, GPS measurements are applied to calibrate the InSAR results and centimeter precision is achieved. As for the ground fissure monitoring, five InSAR cross-sections are designed to demonstrate the relative subsidence difference across ground fissures. In conclusion, the final InSAR subsidence map during 2005–2006 shows four large subsidence zones in Xian hi-tech zones in western, eastern and southern suburbs of Xian City, among which two subsidence cones are newly detected and two ground fissures are deduced to be extended westward in Yuhuazhai subsidence cone. This study shows that the land subsidence and ground fissures are highly correlated spatially and temporally and both are correlated with hi-tech zone construction in Xian during the year of 2005–2006.

Keywords Land subsidence · Ground fissure · SAR interferometry (InSAR) · Monitoring

C. Y. Zhao (✉) · Q. Zhang · C. S. Yang · X. M. Qi
School of Geological Engineering and Geomatics, Chang'an University, Xian, Shaanxi, China
e-mail: zhaochaoying@163.com

X. L. Ding
Department of Land Surveying and Geo-Informatics, Hong Kong Polytechnic University, Hung Hom, Hong Kong, China

Z. Lu
US Geological Survey, Vancouver, WA, USA

Introduction

Xian, the capital city of Shaanxi province, lies in the Weihe Basin northwest of China, where Changan-Lintong fault (CAF Fault hereinafter) in the south of the city is one of the active buried fault, which controls the main geological activities of this region (Peng et al. 1992). Xian has been undergoing serious land subsidence and ground fissures since 1960s. The historical leveling measurements showed that up to 1995, the areas with cumulative subsidence of more than 200 mm were over 145 km^2, and the maximum subsidence was over 2 m. The average ground subsidence rate was 50–100 mm/a, and the maximum rate was up to 300 mm/a. Eight subsidence funnels had been detected in the southern, eastern and southwestern suburbs of Xian City (Yan 1998; Tao 1999). Besides, total 13 ground fissures with similar directions as NNE and approximately parallel each other existed in the subsidence area, which made the subsidence area stretch along ground fissure direction. The total length of ground fissures was over 100 km (Yan 1999; Mi and Zhang 2001; Xian city planning bureau, Institute of geotechnical investigation and design MMI and China Northwest Building Design Research Institute 2006). Figure 1 shows the historical

leveling subsidence contour map up to 1995 in Xian area with the SAR magnitude map as its background, where three rivers as Ba river, Chan river in the east and Zao river in the west of this city, CAF fault in the southern of Xian, 13 ground fissures and confined water contour in 1987 are all overlapped on this map. Besides 24 GPS bench marks installed in 2005 are superimposed in this map for the Synthetic Aperture Radar Interferometry (InSAR) result calibration.

As reported, Xian land subsidence and ground fissure was mainly due to uncontrolled underground water withdrawal, meanwhile CAF fault controlled the location of ground fissures (Wang et al. 1996; Zhang 1990; Wang 2000). The confined water contour map also showed high spatial correlation with land subsidence contour map. Local government had ceased most of wells to decrease the underground water pumping since 1995, as a result the land subsidence rate decreased greatly. However, obvious subsidence was still recorded by step bench mark and three new ground fissures came into being during 2001–2003 (Suo et al. 2005). All these phenomena make the Xian land subsidence and ground fissures be more complex. Unfortunately large scale leveling work has been ceased since 1995, so little information on recent land subsidence and ground fissures activities can be achieved.

InSAR technique was firstly applied for the Venus and Moon surveying (Rogers and Ingalls 1969; Zisk 1972), and in 1986, Seasat SAR data was firstly used for earth surface measurement (Zebker and Goldstein 1986).The first application of differential InSAR was the monitoring of Imperial valley, California (Gabriel et al., 1989).After the ERS1 satellite was launched in 1991,D-InSAR techniques has been widely used to monitor the deformation of earthquake (e.g., Massonnet et al. 1993; Zebker et al. 1994;), volcano (e.g., Lu et al. 2003; Rosen et al. 1996) and land subsidence (e.g., Amelung et al. 1999; Liu et al. 2001). Besides Xian land subsidence evolution have also been researched and high consistency with leveling data have also been achieved (Zhao et al. 2008). The aim of this study is to examine the recent land subsidence and ground fissures deformation using SAR and GPS data. The main subsidence area with 30 × 30 km^2 in ground area will be focused on, which was demonstrated as the whole image of Fig. 1.

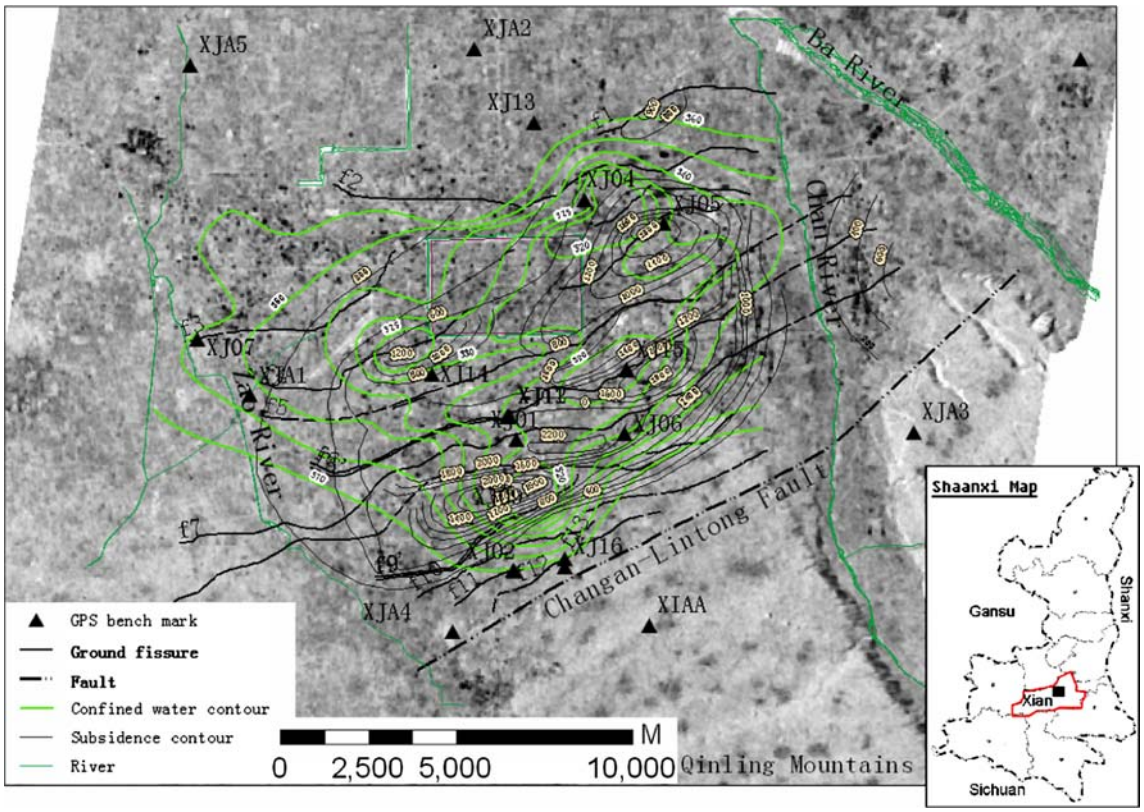

Fig. 1 Location map of Xian City, where three rivers, the CAF fault, 13 ground fissures, contour map of subsidence from leveling measurements from 1959 to 1995, confined water contour in 1987 and GPS stations are superimposed on the SAR magnitude map. The *central rectangle* is Xian ancient city wall. The *inset* is the sketch map of Shaanxi Province, where the *black rectangle* represents the study area

Data introduction

GPS data

GPS networks were installed in 2005, which include 24 bench marks (see Fig. 1), among which six points named as XJA1–XJA6 were set as base points and other 18 points named as XJ01–XJ18 were set as monitoring points. Still the monitoring points could be divided as 11 land subsidence monitoring points and seven ground fissures monitoring points, among which the pairs of XJ02 and XJ03 were at Xian Traffic Police Office of ground fissure f11, the pairs of XJ07 and XJ08 points were at Xian sewage farm of f3 and three points of XJ10, XJ11 and XJ12 were at Chang'an south crossroad of ground fissure f6 and its secondary fissure f6′ (Fig. 7 for details).GPS have been observed biannually since Nov. 2005 and 5 mm vertical precision has been achieved (Zhang et al. 2007).

Envisat data

Seven frames of Envisat ASAR data acquired from the day of January 29, 2005 to April 29, 2006 have been selected in this research. Figure 2 shows the Envisat interferometric datasets pairs, the horizontal line is the SAR acquisition date and the vertical line indicates the length of perpendicular baseline component. Total six interferometric pairs with perpendicular baseline component less than 250 m are shown in this figure in different colors, where each pair is marked by three elements as interferometric number, height ambiguity $h_{2\pi}$ in meters and time spanning in days.

InSAR data processing and their results

Two-orbit method is applied for differential InSAR processing (Massonnet et al. 1993; Massonnet and Feigl 1998), while SRTM DEM with three arc second ground resolution is used as external DEM to subtract the topographic phase. The D-InSAR processing in this research is outlined as follows: firstly aiming to check the SAR data quality, all six pairs of datasets are processed to achieve their differential interferograms. For the investigation of Xian atmospheric effect, the sixth pair data with only 35 days time spanning are taken as an example. Figure 3a and b shows SRTM DEM and differential interferogram of the whole overlapped image respectively, where the red box is the region of interested (ROI), which will be focused on for other pairs of data processing. From the DEM map, the height difference in the ROI is about 200 m, so the height ambiguity must be taken into considerations during the differential processing, especially for the low height ambiguity pairs, such as pair 1 and pair 2 with only 39.3 and 46.6 m height ambiguity respectively. From the differential interferogram, about one-third color cycle deformation can be detected, that is, about 1 cm vertical deformation in 35 days, which will be verified by the other deformation pairs. Besides, no obvious atmospheric fringes from the image 060325 and 060429 can be found, which will be further discussed later.

For the other five interferometric pairs, their interferograms are listed in Fig. 4a–e respectively, while Fig. 4f is the adaptively filtered interferogram of Fig. 4c by using modified Goldstein filtering algorithm (Baran et al. 2003), among which the interfermetric pairs' number and their master and slave image date are superimposed on the above

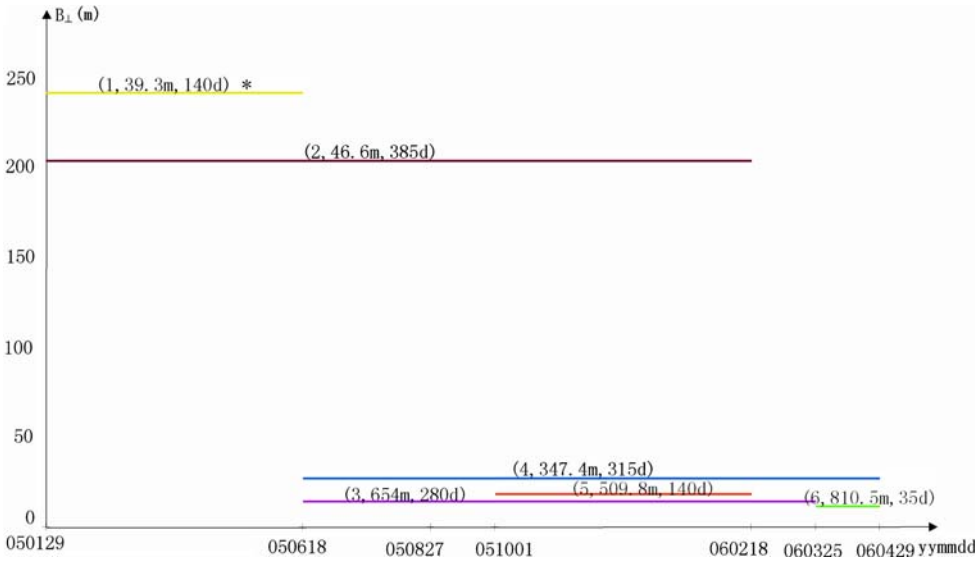

Fig. 2 Envisat ASAR Datasets pairs, where *asterisk* stands for interferometric number, Height ambiguity in meters and time spanning in days

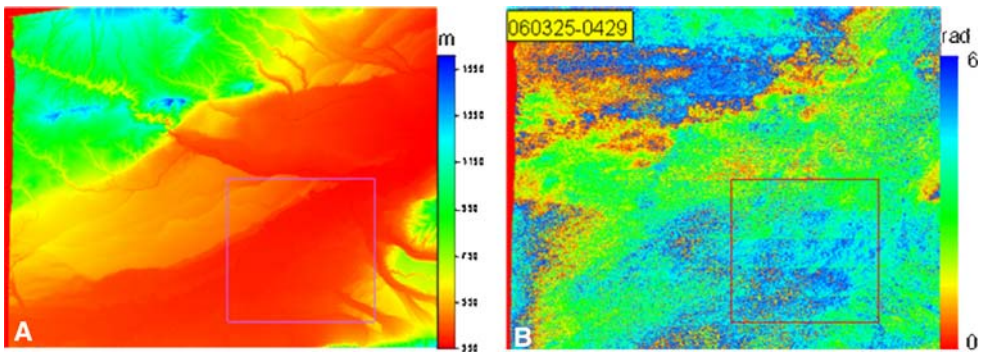

Fig. 3 SRTM DEM map and differential interferogram of pair 6 in Line of sight (LOS) coordinate system, where the *rectangle* is the interested region, which will be focused on by following other datasets. **a** SRTM DEM in LOS and **b** differential Interferogram in LOS of image 060325 and 060429

of each interferograms. Obviously, Fig. 4a–d have similar fringes by considering their different time intervals, but Fig. 4e is different from others. Further, it is found that the image 051001 is only combined to the pair 5 and other six images are all combined in different pairs of dataset at least twice. As mentioned above, interferograms from pairs 1 to 4 and 6 have similar fringes, so the image 051001 is suspicious with inhomogeneous atmospheric effect, therefore the pair 5 will be eliminated for further study. As for the interferograms (a) and (b), it is obvious that both of them suffered heavy noise for the sake of external DEM error and spatial and temporal decorrelation. Exactly to say, the perpendicular baseline of pair 1 is up to 250 m and the time span of pair 2 is up to 385 days, so these two pairs of data are also cancelled.

For the subsidence calculation, both pair 3 and pair 4 are applied for following reasons: firstly they have approximate time spans with nearly 1 year as 280 days and 315 days respectively, which is reasonable to compare their D-InSAR results each other and to calculate annual subsidence rate. Secondly both interferometric pairs have so short perpendicular baseline as 14.5 and 27.3 m respectively that external DEM error and baseline decorrelation can be omitted at all. Lastly both pairs have the same master image as 050618 and their slave images have no significant atmospheric effects which have been verified before by the interferogram of pair 6 shown in Fig. 3b. On the other hand, as for the ground fissures deformation monitoring is mainly focused on in this research, so the heavy interferogram filtering is not applied for the loss of deformation resolution shown in Fig. 4f. Figure 5a and b shows the geocoded annual vertical deformation maps of pair 3 and 4 respectively, where the subsidence areas and subsidence rates are consistent greatly. Next in order to mitigate the stochastic error, two subsidence maps are weighted averaged by using their coherence values to achieve the final annual subsidence map during 2005–2006, which are shown in Fig. 6, where also GPS bench

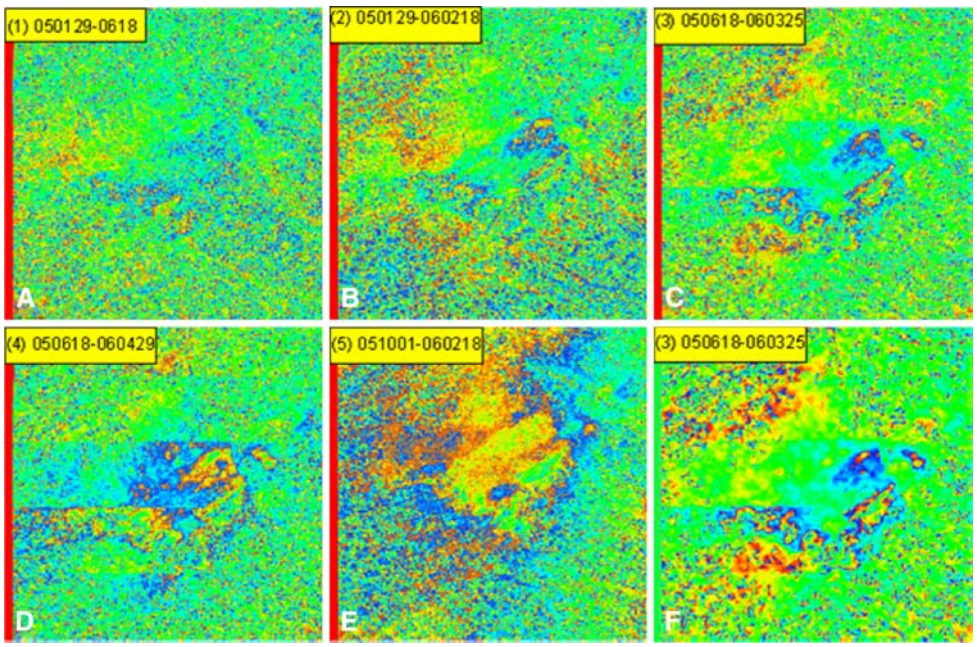

Fig. 4 Differential SAR interferograms of Pairs 1–5 as (**a–e**) respectively and the (**f**) is the adaptively filtered interferogram of (**c**)

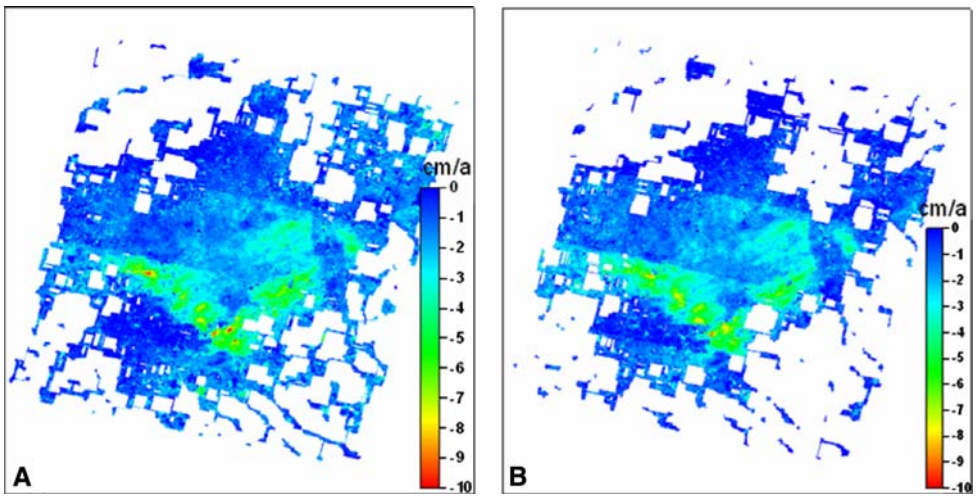

Fig. 5 Annual subsidence rate maps of pairs 3 and 4 in (**a**) and (**b**) respectively, which have the same color bar scaled as 0 to −10 cm/a

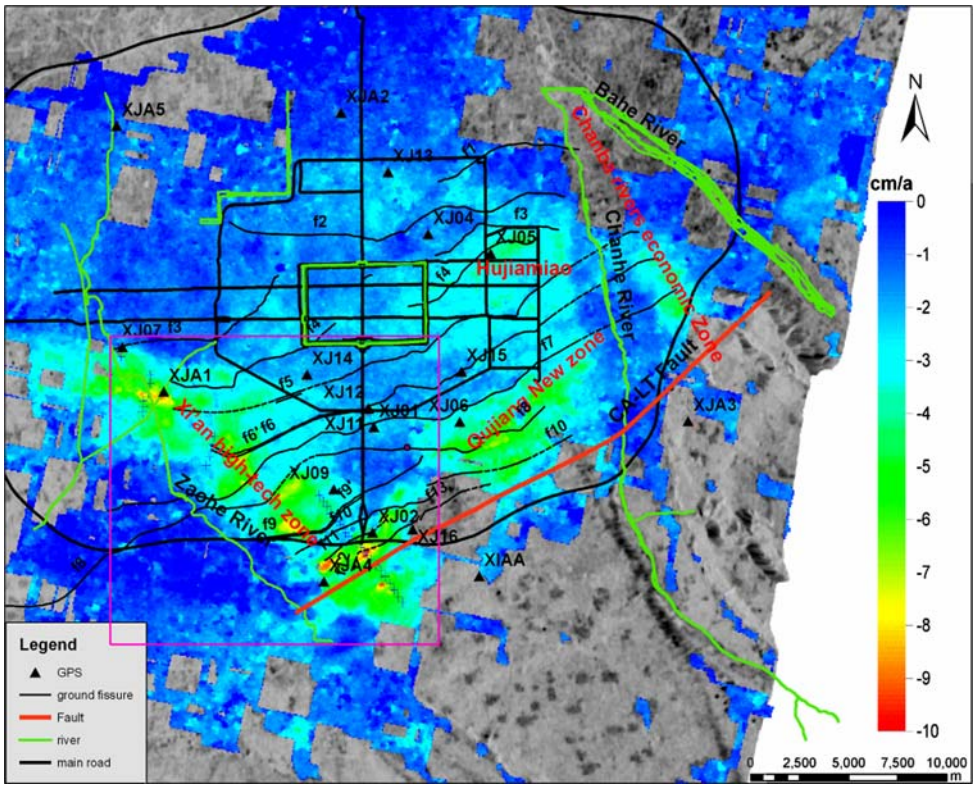

Fig. 6 InSAR annual subsidence rate map during June 2005–June 2006

marks, ground fissures, CAF fault, main rivers and roads are all overlapped. The InSAR results at 19 discrete GPS points are abstracted and listed in Table 1.

In order to research the deformation of ground fissures in new subsidence region of Xian hi-tech zone, an enlarged map marked with pink rectangle at the bottom left of Fig. 6 is shown in Fig. 7, where five profiles named as AA′, B1B1′, B2B2′, CC′, DD′ at CAF Fault and different ground fissures are marked, and the inset is a photo of Chang'an south crossroad section taken in 1996 (Wang 2000). Exactly to say the profile AA′ crossing CAF Fault, f12,f11,f10,f9′−f9 aim to detect the displacement crossing these ground fissures. The profiles B1B1′ and B2B2′ aim to detect the subsidence differences of f6−f6′ at Tangyan road and Chang'an south crossroad respectively, also 3 GPS bench marks installed at Chang'an south crossroad for the ground fissure monitoring can be applied to verify the InSAR monitoring ability. The profile CC′ at the west of the west ends of f4 and f5 aim to deduce the exact fissure locations. The profile DD′ at Xian sewage farm at the west

end of f3 aim to check the ground fissure monitoring ability between GPS and InSAR, where two GPS points as XJ07 and XJ08 were installed, and the distances of GPS points and f3 are only in 10 m apart. These five profiles are mapped in the Fig. 8a–d, where the location of fault and fissures are also approximately indicated.

Table 1 The comparison of annual subsidence rates at GPS points between InSAR and GPS results

No.	Name	GPS (cm/a)	InSAR (cm/a)	Residual (cm/a)
1	XJA1	−7.6	−8	−0.4
2	XJA2	−1.2	−1.3	−0.1
4	XJA4	−2.1	−2.2	−0.1
5	XJA5	−0.9	−0.9	0
6	XJA6	−0.8	−0.7	0.1
7	XJ01	−0.9	−1.9	−1
8	XJ02[a]	−4.6	−5.6	−1
9	XJ03[a]	−2	−3.9	−1.9
10	XJ04	−1	−2	−1
11	XJ05	−3.7	−3.9	−0.2
12	XJ06	−2.6	−3.3	−0.7
13	XJ07[a]	−3.4	−3.7	−0.3
14	XJ08[a]	−1.9	−3.1	−1.2
16	XJ10[a]	−2.3	−2.4	−0.1
17	XJ11[a]	−3.6	−2.3	1.3
18	XJ12[a]	−2.1	−2.4	−0.3
19	XJ13	−3.2	−2	1.2
20	XJ14	−3.8	−2	1.8

[a] Ground fissure monitoring bench mark

Discussions

Subsidence monitoring

By comparing GPS and InSAR results in this research, it can be seen that the centimeter precision of differential InSAR results can be achieved by selecting the rational interferometric pairs to mitigate the baseline decorelation and atmospheric effect etc. If the GPS points near ground fissure field were excluded, the InSAR precision should be increased in some extent. Secondly, from the land subsidence map (see Fig. 6), four large subsidence zones can be obviously detected as Xian hi-tech zone, Xian Qujiang new zone, Chanba rivers economic zone and Hujiamiao area. The former three zones are newly constructed after 1996 or 2000 or so, while Hujiamiao is one of the eight subsidence cones detected from the historical leveling results and it is continuously subside up to date. The mean subsidence rate in each subsidence zones is about 6 cm/a, and the maximum rate is up to 10 cm/a at Traffic Police Office and Yuhuazhai at Xian hi-tech zones. On the other hand, the newly detected ground fissures of f11 and f12 are just located at the Traffic Police Office area (see Fig. 7). So

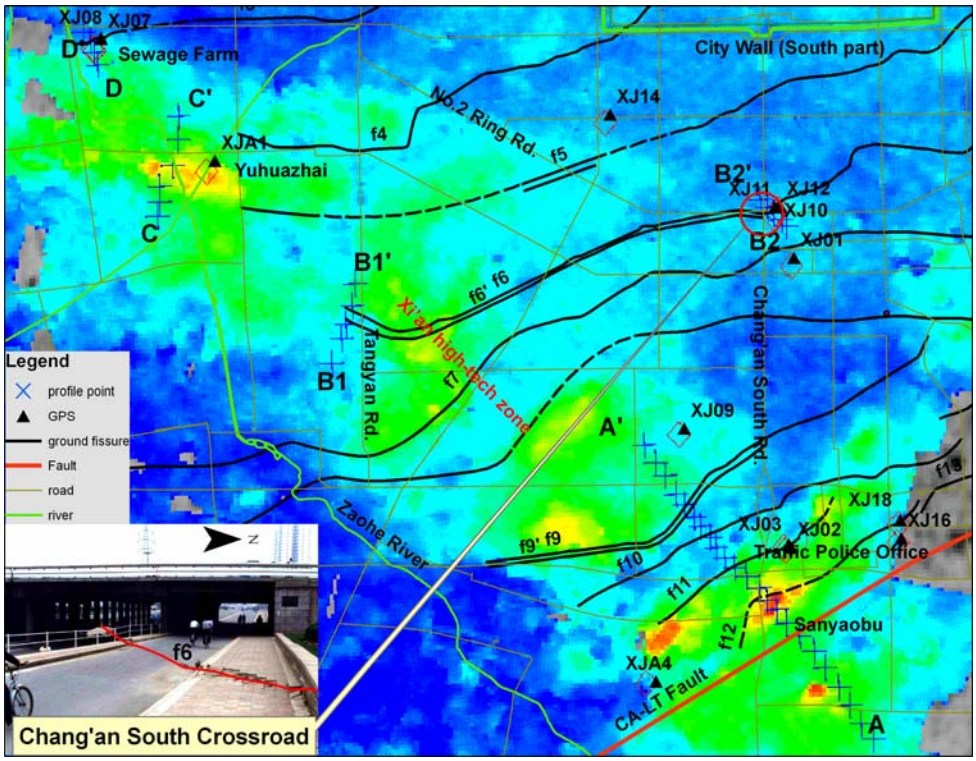

Fig. 7 The enlarged InSAR annual subsidence rate map in Xian hi-tech zone, where five ground fissure profiles are marked, the inset is a photo of fissure f6 at Chang'an south crossroad taken in 1996

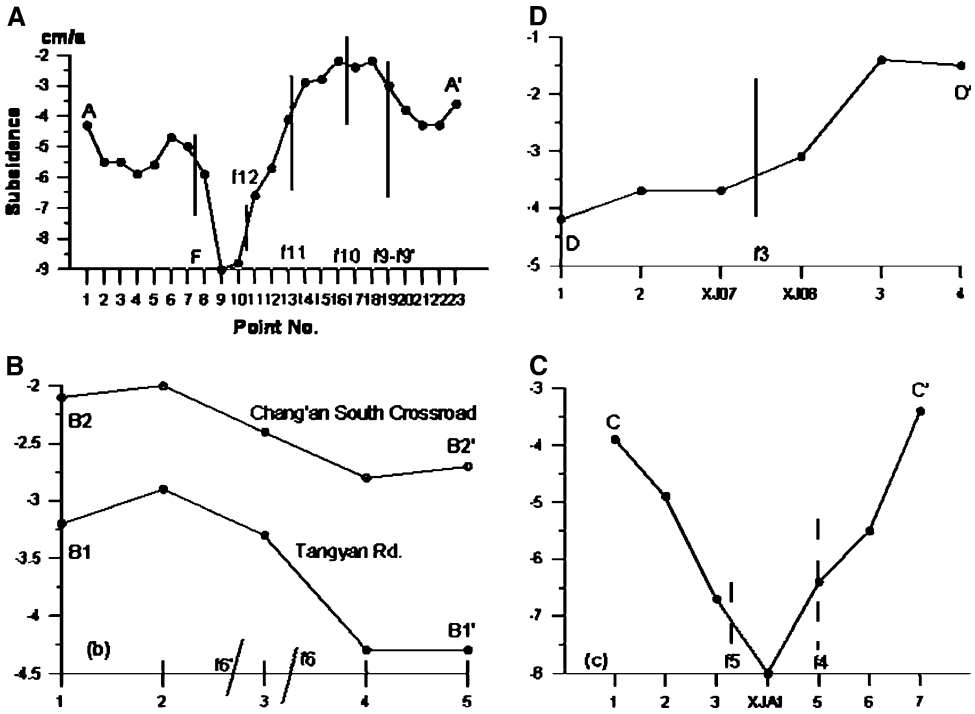

Fig. 8 Profiles of different subsidence crossing fault and different ground fissures. **a** Profile crossing CAF fault, f12, f11, f10, and f9-f′9 at Traffic Police Office section, **b** profiles crossing f6-f6′ at Chang'an south crossroad and Tangyan road respectively, **c** profile crossing f4 and f5 at their west ends, where both fissures have been extended westwards and **d** profile crossing f3 at Xian sewage farm

again it can be drawn that the ground fissure and land subsidence have high spatial and temporal correlations.

Ground fissures monitoring

As far as the ground fissure monitoring is concerned, InSAR technique shows the great ability to detect the subsidence differences across the fissures. Firstly, profile AA′ in Fig. 8a shows that CAF fault, f12, f11 and f9−f9′ are greatly active during this period, while the deformation magnitude of fault is up to 1 cm and the newly detected fissures f12 and f11 have 2 cm and 3 cm displacement respectively. Meanwhile the GPS results at XJ02 and XJ03 points also indicate the 2.6 cm subsidence difference listed in Table 1 for the f11 monitoring, so these two techniques can give consistent results in ground fissure detection at this section. Secondly, two short profiles named as B1B1′ and B2B2′ across f6 −f6′ at Tangyan road and Chang'an south crossroad respectively shown in Fig. 8b demonstrate the different activities of fissure f6 at different sections. Exactly to say, f6 at Chang'an South Crossroad is not active during 2005–2006, which can also be verified by GPS measurements at points XJ10,XJ11 and XJ12 listed in Table 1, but in 1996 it was greatly active, which can be seen from the picture at the bottom left of Fig. 7. On the other hand, the fissure f6 at Tangyan road in Xian hi-tech zone is greatly active during the monitoring period and the maximum subsidence difference is up to 1 cm/a, while it did not exist at all before the hi-tech construction in 1996. Thirdly, the profile CC′ located at the extent area of the westward of fissures f4 and f5 at Yuhuazhai area, where one of GPS bench mark XJA1 was installed as base point originally. Actually both GPS and InSAR results show the great land subsidence in this region, the maximum subsidence amounts to 8 cm/a. Figure 8c shows great subsidence difference, where the dashed line denotes the deduced or burred ground fissures. Lastly, in order to check the ability for ground fissure monitoring of GPS and InSAR techniques, especially for the ground fissure influenced zone detection, the profile DD′ of f3 at Xian sewage farm is demonstrated at Fig. 8d, where two GPS bench marks named XJ07 and XJ08 installed in the extent of 10 m apart from f3. The GPS results from Table 1 show 1.5 cm subsidence difference during this period, however the InSAR results at these two points in Fig. 8d show only millimeters subsidence differences and InSAR results of other 4 points far away from GPS bench marks can show the same magnitude of subsidence difference as GPS do. So it is clear to see GPS is super to InSAR for the influenced area monitoring of active ground fissure. The main cause is the low resolution of InSAR results of Envisat data. Even so InSAR technique can be applied to detect the approximate locations and directions of ground fissures.

Conclusions and perspectives

InSAR technique has been successfully applied to detect the Xian land subsidence and ground fissures deformation during 2005–2006. And following conclusions can be drawn. In order to achieve robust InSAR results, several InSAR errors as temporal decorrelation, baseline decorrelation, external

DEM error, atmospheric effect should be taken into considerations. In this paper, 6 pairs of InSAR data are processed and their interferograms are compared, so the errors mentioned above are eliminated or mitigated by selecting rational datasets and weighted average their subsidence results. Therefore the precision of final annual subsidence results from InSAR is about centimeter which can be calibrated with GPS measurements during the same period. Followed from the subsidence map, four main land subsidence zones have been clearly detected as Xian hi-tech zone, Qujiang New zone, Chanba rivers economic zone and Hujiamiao with their mean subsidence rate as 6 cm/a during the years of 2005–2006, while the former three zones are newly detected. Still two new subsidence cones in Xian hi-tech zone named as Yuhuazhai and Sanyaobu with maximum subsidence as 10 cm/a are firstly discovered. On the other hand, the monitoring of ground fissure is also analyzed by InSAR technique. Five cross-sections of InSAR results crossing ground fissures show that about centimeter subsidence difference can be detected, so Xian ground fissures activities are investigated during 2005–2006, which are beneficial to scientists and local government for research and mitigation of ground fissures damage. However, the exact influenced areas of ground fissure cannot be detected from differential InSAR technique for the low resolution sake up to date, while GPS is a complementary method. From InSAR monitoring results, the fissures of f4 and f5 are deduced to be extended westward at Yuhuazhai to the east bank of Zaohe river, which should be verified by field investigation.

In Xian, the land subsidence and ground fissures are highly correlated spatially and temporally and both are correlated with the hi-tech zone construction. In order to increase the ground fissure monitoring ability, the new SAR data as TerraSAR X or COSMO sky/med data should be tested. And new InSAR techniques as Permanent Scatters (PS) and Corner Reflector (CR) InSAR are good at errors mitigation and ground fissures detection respectively. Lastly the new findings of the subsidence cones and ground fissure displacement in this research should be further verified by future research and field exploration.

Acknowledgments Envisat ASAR data are provided by ESA Category 1 and this research is funded by two general projects of the Natural Science Foundation of China (NSFC) (project No: 40672173 and 40802075) and one key project of the Ministry of Land & Resources, China (project No: 1212010440410), and above all special thanks to the reviewer of this paper for his helpful comments.

References

Amelung F, Galloway DL, Bell JW, Zebker HA, Laczniak RJ (1999) Sensing the ups and downs of Las Vegas: InSAR reveals structural control of land subsidence and aquifer-system deformation. Geology 27(6):483–486

Baran I, Stewart M, Kampes B, Perski Z, Lilly P (2003) A modification to the Goldstein radar interferogram filter. IEEE Trans Geosci Remote Sens 41(9):2114–2118

Gabriel AK, Goldstein RM, Zebker HA (1989) Mapping small elevation changes over large areas: differential radar interferometry. J Geophys Res 94:9183–9191

Liu GX, Ding XL, Chen YQ, Li ZL, Li ZW (2001) Settlement field of Chek Lap Kok airport, HongKong, detected by satellite synthetic aperture radar interferometry. Chin Sci Bull 46:1778–1782

Lu Z, Patrick M, Fielding EJ, Trautwein C (2003) Lava volume from the 1997 eruption of Okmok volcano, Alaska, estimated from spaceborne and airborne interferometric synthetic aperture radar. IEEE Trans Geosci Remote Sens 41:1428–1436

Massonnet D, Feigl KL (1998) Radar interferometry and its application to changes in the Earth's surface. Rev Geophys 36:441–500

Massonnet D, Rossi M, Carmona C, Adragna F, Peltzer G, Feigl K, Rabaute T (1993) The displacement field of the Landers earthquake mapped by radar interferometry. Nature 364(6433):138–142

Mi FS, Zhang ZX (2001) Disasters of Xian ground fissures and controlling measures. Res Soil Water Conserv 18(1):155–159

Peng JB, Su SR, Zhang J (1992) The active faults and geohazards in Weihe basin. Northwest university Press, Xian

Rogers AEE, Ingalls RP (1969) Venus: mapping the surface reflectivity by radar interferometry. Science 165(3895):797–799

Rosen P, Hensley SH, Zebker H, Webb FH, Fielding EJ (1996) Surface deformation and coherence measurements of Kilauea volcano, Hawaii, from SIR-C radar interferometry. J Geophys Res 101:23109–23125

Suo CM, Wang DQ, Liu ZZ (2005) Land fracture and subsidence prevention in Xian. Quat Res 25(1):23–28

Tao H (1999) The land subsidence map in Xian city, in Shaanxi Geology and minerals resources bureau, Shaanxi proposal committee. Xian environmental geological Atlas. Xian Mapping Press, Xian

Wang DQ, Suo CM, Jia SJ (1996) A quantitative analysis of recently extraordinary movement factors of geofractures in Xian. Geol Shaanxi 14(1):49–58

Wang JM (2000) Theory of ground fissures hazards and its application. Shaanxi Science and Technology Press, Xian

Xian city planning bureau, Institute of geotechnical investigation and design MMI and China Northwest Building Design Research Institute (2006) Regulations of field reconnaissance and engineering design on Xian ground fissures, No. DBJ61-6-2006

Yan WZ (1998) Analysis on the origin of land subsidence and its countermeasures of control in Xian. Chin J Geol Hazard Control 119:27–32

Yan WZ (1999) Xian ground fissures map, in Shaanxi Geology and minerals resources bureau, Shaanxi proposal committee, Xian Environmental geological Atlas. Xian Mapping press, Xian

Zebker HA, Goldstein RM (1986) Topographic mapping from interferometric synthetic aperture radar observations. J Geophys Res 91(B5):4993–4999

Zebker HA, Rosen PA, Goldstein RM, Gabriel A, Werner CL (1994) On the derivation of coseismic displacement fields using differential radar interferometry: the Landers earthquake. J Geogr Res 99:19617–19634

Zhang JM (1990) Research on ground fracture in the region of Xian. Northwest University Press, Xian

Zhang Q, Huang GW, Wang L, Wu XZ, Ding XG (2007) Applied research of monitoring the Xian land subsidence and land fissure using GPS surveying (in Chinese). J Eng Geol 6(15):P828–P833

Zhao CY, Ding XL, Zhang Q, Lu Z, Li ZW (2008) Monitoring of recent land subsidence and ground fissures in Xi'an With SAR interferometry, ISPRS proceedings 2008 Beijing, B1, TCI,pp 147–150

Zisk SH (1972) A new Earth-based radar technique for the measurement of lunar topography. Moon 4:296–300